ACS APPLIED MATERIALS & INTERFACES

Research Article

www.acsami.org

From Azo-Linked Polymers to Microporous Heteroatom-Doped Carbons: Tailored Chemical and Textural Properties for Gas Separation

Babak Ashourirad, Pezhman Arab, Alyson Verlander, and Hani M. El-Kaderi*

Department of Chemistry, Virginia Commonwealth University, Richmond, Virginia 23284-2006, United States

Supporting Information

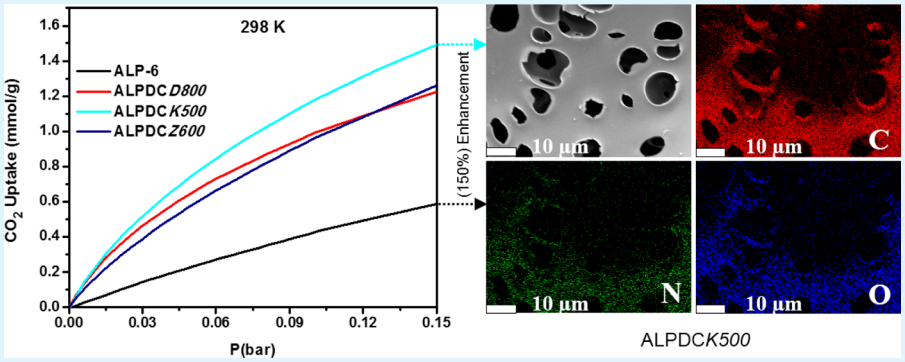

ABSTRACT: Heteroatom-doped porous carbons with ultrahigh microporosity were prepared from a nitrogen-rich azo-linked polymer (ALP-6) as a precursor for gas separation applications. Direct carbonization and chemical activation of ALP-6 with $ZnCl_2$ and KOH were successfully applied to obtain three different classes of porous carbons (ALPDCs). Synthetic processes were conducted at relatively mild temperatures (500−800 °C),which resulted in retention of appreciable levels of nitrogen content (4.7−14.3 wt %). Additionally, oxygen functionalities were found to be present in chemically activated samples. The resultant porous carbons feature a diverse range of textural properties with a predominant microporous nature in common. The highest CO_2 uptake value of 5.2 mmol g^{-1} at 1 bar and 298 K in ALPDCK600 was originated from well-developed porosity and basic heteroatoms (N and O) on the pore walls. The highest heteroatom doping level (12 wt % nitrogen and 20 wt % oxygen) coupled with the high level of microporosity (84%) for ALPDCK500 led to notable CO_2/N_2 (62) and CO_2/CH_4 (11) selectivity values and a high CO_2 uptake capacity (1.5 mmol g^{-1}, at 0.15 bar) at 298 K. This study illustrates the effective use of a single-source precursor with robust nitrogen bonds in combination with diverse carbonization methods to tailor the chemical and textural properties of heteroatom-doped porous carbons for CO_2 capture and separation applications.

KEYWORDS: *heteroatom-doped carbons, carbonization, CO_2 adsorption, azo-linked polymers, gas separation*

INTRODUCTION

Global climate change has become a serious concern for human beings and ecosystems because of the emission of greenhouse gases (GHGs), such as CO_2, CH_4, and NO_x.[1] In particular, the drastic increase in CO_2 concentration caused by burning fossil fuels for energy generation contributes significantly to the GHG effect.[2,3] Since the world energy demands will continue to depend on fossil fuels in the foreseeable future, the carbon dioxide capture and sequestration (CCS) has emerged as an absolute necessity for environment protection.[4] Thus, great efforts have been devoted to developing materials and technologies for efficient CO_2 capture.[5] The acidic nature of CO_2 allows for chemical absorption by amine solutions thanks to their basic sites. Appropriately, liquid amine scrubbing technology involving aqueous monoethanolamine (MEA) solution has been widely employed by industry for CO_2 capture technology despite its drawbacks.[6] Because of the chemical bonding of CO_2 by such solutions, considerable amount of energy is required for solvent regeneration. Furthermore, chemical decomposition, evaporation, and corrosion of amine solutions limit their applications. To overcome the huge energy penalty for the regeneration-absorption and other disadvantages of amine solutions, physical adsorption by porous solids has been developed as an alternative approach during the past decade.[7,8] The physically adsorbed CO_2 molecules on the pore walls of solid sorbents can be easily regenerated by vacuum swing or pressure swing processes.[9]

Among many CO_2 sorbents investigated so far, activated carbons attracted considerable attention because of their fascinating features such as hydrophobicity, physicochemical stability, low density, controllable porosity, and adjustable

Received: January 15, 2016
Accepted: March 14, 2016
Published: March 14, 2016

DOI: 10.1021/acsami.6b00567
ACS Appl. Mater. Interfaces 2016, 8, 8491−8501

Scheme 1. Schematic Representation of the Synthesis of ALP-6 Derived Carbons

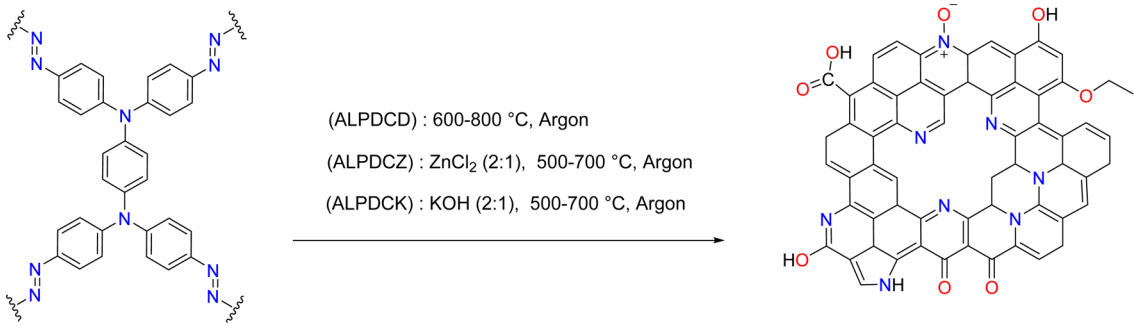

chemical functionality. Despite the mass production and commercialization of activated carbons, it is desired to further enhance the key uptake features such as adsorption capacity and selectivity. Accordingly, nitrogen as one of the most widely researched heteroatom dopants can induce simultaneous high CO_2 capture capacity and selectivity of carbon materials. Lewis acid−base interaction between acidic CO_2 molecules and basic nitrogen moieties on the pore walls of carbon provides efficient adsorption capacity.[10−12] Moreover, the activation (chemical or physical) and carbonization of carbon precursors have been proven to improve the CO_2 uptake through the generation of narrow pores.[13−16] It is therefore of great importance to generate high performance nanoporous carbons which benefit from both narrow microporosity and nitrogen basic heteroatoms. This can be fulfilled by selecting a single source precursor that contains both C and N followed by a one-step carbonization and/or activation process.[17]

Recently, major efforts have been devoted to the development of task-specific single-source precursors of carbon and desired heteroatom (nitrogen) to be used for subsequent carbonization-activation. Accordingly, various promising single sources of nitrogen and carbon including nitrogen-decorated metal−organic-frameworks (ZIF-8),[18,19] nitrogen containing porous organic polymers (imine-linked,[20,21] benizimidazole-linked[17] and hypercross-linked polymers[22]), ionic liquids,[23,24] metal salts,[25,26] and biomasses[27,28] have been successfully transformed to N-doped carbons. However, the elimination of heteroatoms upon high temperature treatment results in a low dopant level in the final product and low selective adsorption of CO_2 over CH_4 and N_2. It is therefore, highly desirable to develop a precursor with intrinsically robust nitrogen functionalities that can be retained in the final structure of the porous carbons. Additionally, employing precursors with initial porosity and nitrogen-containing groups, which are able to undergo both direct carbonization and chemical activation to yield N-doped porous carbons, has been rarely studied.[22] From a synthetic point of view, although the KOH-activation has been applied to a vast range of precursors, the use of $ZnCl_2$ has been limited to biomasses.[29] Such challenges have not been addressed and discussed sufficiently in the literature.

With these considerations in mind, we introduce new families of heteroatom-doped porous carbons by using an azo-linked polymer (ALP-6) as a novel precursor and chemical activation/direct carbonization as one-step synthesis platforms. The task-specific ALP-6 precursor has a high nitrogen content (14.7 wt %) and porosity (SA_{BET}= 800 m^2 g^{-1}). On the basis of these features of ALP-6, direct carbonization and chemical activation with $ZnCl_2$ and KOH were applied to obtain three different classes of ALP-6 derived carbons (ALPDCD, ALPDCZ, and ALPDCK, respectively). Notably, the highly stable nitrogen−nitrogen linkages in ALP-6 structure will benefit high doping level of heteroatoms in all carbons. One of the carbons successfully retained an exceptionally high portion (96%) of the original nitrogen atoms. Textural properties, surface chemistry, gas adsorption, and selectivity of prepared carbons along with ALP-6 were comparatively investigated. In general, we demonstrate that controlled activation and carbonization of a precursor with intrinsically robust nitrogen functionalities allow for development of microporous doped-carbons with simultaneous high CO_2 uptake capacities as well as CO_2/N_2 and CO_2/CH_4 selectivity values.

EXPERIMENTAL SECTION

Materials. All starting materials and solvents were obtained from commercial sources and used without further purification. KOH (Alfa Aesar, ACS, 85% min, K_2CO_3 2.0% max pellets) and $ZnCl_2$ (Alfa Aesar, anhydrous, 98+%) were stored in a glovebox and used as received. *N,N,N′,N′*-tetrakis (4-aminophenyl)-1,4-phenylenediamine was purchased from Combi-Blocks.

Preparation of ALPDCs. The single source precursor, ALP-6, was synthesized through copper(I)-catalyzed oxidative homocoupling of *N,N,N′,N′*-tetrakis (4-aminophenyl)-1,4-phenylenediamine monomer following the procedure we recently reported.[30] ALP-6 batches were combined (∼3.0 g) and outgassed at 120 °C and 150 mTor for 24 h. The first class of porous carbons was synthesized by direct carbonization of ALP-6. In a typical synthesis, 300 mg of outgassed ALP-6 was placed in a ceramic boat then directly heated to the targeted temperatures of 600, 700, and 800 °C with a heating rate of 5 °C/min under ultrahigh purity Ar flow and held for 1 h at the desired temperature. ALP-6 derived carbons synthesized by this procedure were labeled as ALPDC*DT*, where *D* and *T* represent direct pyrolysis and the targeted carbonization temperature, respectively. The second and third classes of porous carbons were synthesized by pyrolysis of ALP-6 after activation with KOH and $ZnCl_2$, respectively. In a typical procedure, 400 mg of activated ALP-6 precursor was thoroughly mixed with 800 mg of KOH or $ZnCl_2$ (2:1 weight ratio of activating agent to polymer). To minimize the effect of water absorption on the surface of activated polymers and reaction with activation agents, this step was carried out under nitrogen inside a glovebox. The uniform powder mixture obtained by physical mixing and grinding was placed in a boat then transferred to a tube furnace and heated up to 500, 600, and 700 °C as discussed above. After cooling to room temperature, the black carbon samples were soaked and washed three times with HCl (1.0 M) to remove unreacted KOH, $ZnCl_2$ or residual salts. Further purification was performed by washing with distilled water and ethanol, respectively. The resulting activated carbons were dried under vacuum at 200 °C for 12 h. These classes of ALP-6 derived carbons were denoted as ALPDC*KT* and APLDC*ZT* in which, *K*, *Z* and *T* represent chemical activation by KOH, $ZnCl_2$ and activation

DOI: 10.1021/acsami.6b00567
ACS Appl. Mater. Interfaces 2016, 8, 8491−8501

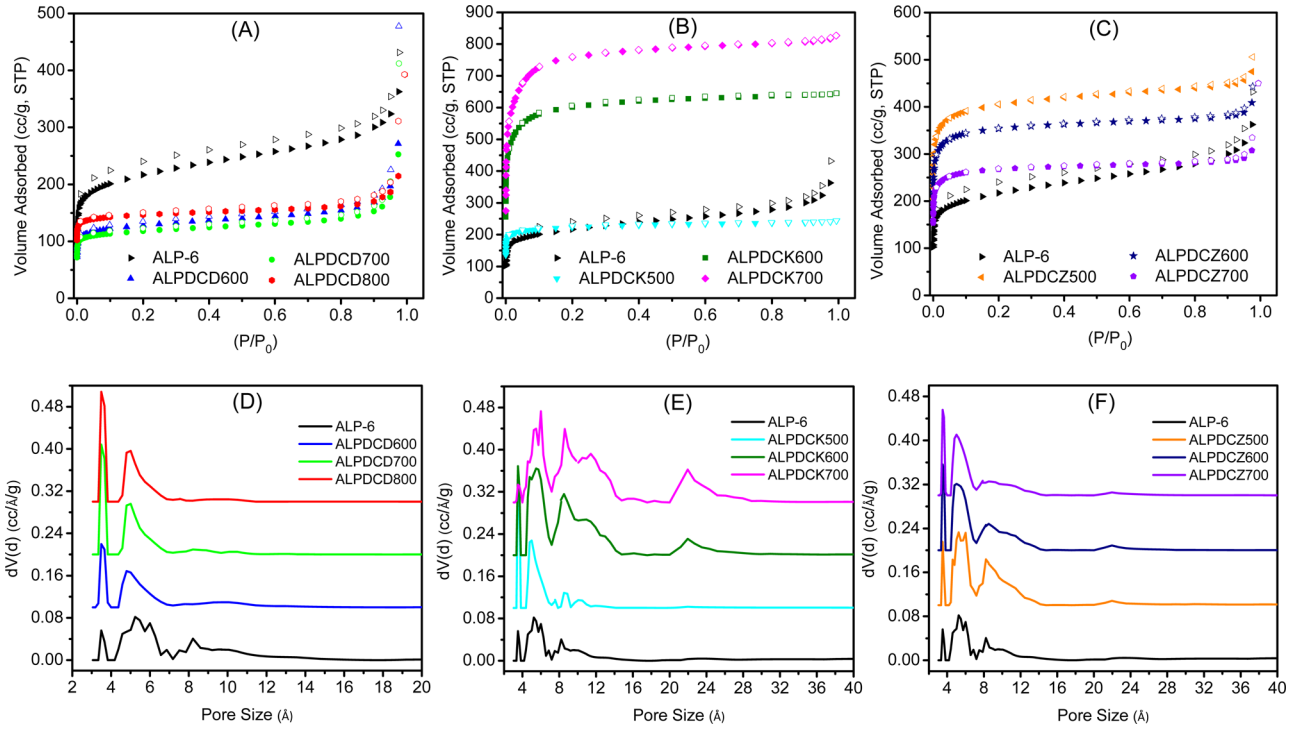

Figure 1. (A–C) Nitrogen isotherms at 77 K and (D-F) pore size distributions calculated by DFT method for ALP-6 derived carbons and ALP-6 precursor (All PSD curves are offset vertically in steps of 0.1 for clarity).

temperature, respectively. Synthetic routes of porous carbons are depicted in Scheme 1.

Measurements and Characterization for ALPDCs. Gas adsorption isotherms for N_2 (at 77, 273, and 298 K), CO_2 (at 273 and 298 K), and CH_4 (at 273 and 298 K) were measured on Autosorb-iQ2 volumetric adsorption analyzers (Quantachrome Inc.) using ultrahigh purity grade adsorbates. Before adsorption measurements, each sample was degassed under vacuum for at least 12 h at 200 °C. The specific surface area of the samples was measured using the Brunauer–Emmett–Teller (BET) method. Incremental pore size distributions (PSD) were obtained from adsorption branch of N_2 (at 77 K) isotherms by the QSDFT (quench solid density functional theory) method as well as adsorption branch of CO_2 (at 273 K) isotherms by the NLDFT (non-local density functional theory) method assuming slit-like geometry on the carbon material kernel. The volume of micropores (V_{Mic}) was estimated by cumulative pore size distribution curves and corresponding volume at pore size of 2 nm. As a control, *t*-plot method provided by Quantachrome was also utilized to confirm V_{Mic} obtained by PSD curves. The volume of ultramicropores (V_0) was estimated from CO_2 (273 K) isotherms after adjustment of CO_2 pressure at 273 K. Scanning electron microscopy (SEM) images were obtained using a Hitachi SU-70 scanning electron microscope. The samples were prepared by dispersing each specimen onto the surface of a sticky carbon attached to a flat aluminum sample holder. Then the samples were coated with platinum at a pressure of 10^{-5} mbar in a N_2 atmosphere for 60 s before SEM imaging. Elemental analyses of carbon, nitrogen, hydrogen, and ash were performed at the Midwest Microlab, LLC. The X-ray photoelectron spectroscopy (XPS) analysis was performed on a Thermo Fisher Scientific ESCALAB 250 spectrometer employing Al Kα (1486.68 eV) X-ray source equipped with a hemispherical analyzer. To prepare the samples for XPS measurements, the carbon specimen was pressed into a piece of indium foil, which was mounted on the sample holder using a double-sided sticky tape. During XPS analysis, a combination of a low-energy electron flood gun and an argon ion flood gun was utilized for charge compensation. The binding energy scale was calibrated by setting the C 1s peak at 285.0 eV. The XPS data were analyzed with Thermo Avantage software (v4.84).

RESULTS AND DISCUSSION

Textural Properties. Nitrogen sorption measurements were carried out to investigate the porosity of ALP-6 derived porous carbons. The BET equation was applied to the N_2 adsorption isotherms to obtain the surface area where the P/P_0 range was chosen by micropore BET assistant software to yield a high R^2 value and a positive line intersect of multipoint BET fitting (Figure S1). To compare the porosity levels, nitrogen isotherms for each class of prepared carbons were stacked along with isotherm of ALP-6 in a separate graph as illustrated in Figures 1A–C. Consistent with most of the porous organic polymers, ALP-6 exhibits type I/IV isotherm with a notable hysteresis loop at P/P_0 = 0.2–0.8 that vanishes upon carbonization. According to Figures 1A–C direct carbonized samples show lower uptakes with respect to ALP-6, whereas, activated carbons feature enhanced uptakes. The nitrogen adsorption isotherms of all ALP-6 derived carbons can be classified as type I with a sharp uptake at low partial pressure region (P/P_0 < 0.01) followed by a plateau for most of the remaining pressure range, which is indicative of microporosity. Compared with the BET surface area of ALP-6 (800 $m^2\ g^{-1}$), the BET surface areas of ALPDCD600, ALPDCD700, and ALPDCD800 drop to 489, 458, and 582 $m^2\ g^{-1}$, respectively. This drop in porosity level is most likely driven by the collapse of the pores and the lack of activation mechanisms during direct carbonization process. In contrast, the surface areas of KOH-activated carbons found to be 881, 2347, and 2952 $m^2\ g^{-1}$ for ALPDCK500, ALPDCK600, and ALPDCK700, respectively. The ALPDCK500 sample features almost an identical surface area to the pristine polymer; however, the nature of porosity in these two materials is different. The type I nitrogen isotherm of ALPDCK500 (Figure 1 B), as well as the numerical values for micropore and ultramicropore volume (V_{Mic} and V_0 in Table 3) clearly indicate that unlike ALP-6 this

DOI: 10.1021/acsami.6b00567
ACS Appl. Mater. Interfaces 2016, 8, 8491–8501

Table 1. Textural Properties of ALP-6 Derived Carbons and ALP-6

	textural properties				
sample	S_{BET} [a] (m^2 g^{-1})	V_{Tot} [b] (cm^3 g^{-1})	V_{Mic} [c] (cm^3 g^{-1})	V_{Mic} [d] (cm^3 g^{-1})	V_0 [e] (cm^3 g^{-1})
ALP-6	803	0.50	0.23 (46)	0.23	0.14
ALPDCD600	489	0.31	0.16 (52)	0.16	0.12
ALPDCD700	458	0.28	0.15 (54)	0.15	0.12
ALPDCD800	582	0.29	0.20 (69)	0.20	0.15
ALPDCK500	881	0.37	0.31 (84)	0.32	0.22
ALPDCK600	2347	0.99	0.77 (78)	0.84	0.35
ALPDCK700	2952	1.26	0.90 (71)	1.0	0.30
ALPDCZ500	1585	0.71	0.54 (76)	0.56	0.26
ALPDCZ600	1395	0.60	0.48 (80)	0.50	0.25
ALPDCZ700	1057	0.45	0.37 (82)	0.37	0.21

[a]Calculated in the partial pressure range which gives the best linear fitting. [b]Total pore volume at P/P_o = 0.95. [c]Determined by cumulative pore volume and maxima of the PSD assuming slit-shaped pores and QSDFT model; the values in parentheses are the percentage of micropores volume relative to total pore volume. [d]Evaluated by the *t*-plot method. [e]Pore volume of ultramicropores (<0.7 nm) obtained from CO_2 adsorption data at 273 K.

carbon sample is mainly composed of fine micropores. The significant enhancement of surface area for samples synthesized at higher temperatures (600 and 700 °C) can be correlated to the higher degree of activation achieved by KOH through several consecutive mechanisms such as etching (by redox reactions), gasification (by evolving gaseous species such as CO and CO_2) and expansion (by metallic potassium) of carbon framework.[10] The use of higher activation temperatures also leads to narrow mesopore formation as evidenced by the broadening of the N_2 isotherms knees at relatively low pressures as well as pore size distribution studies as we discuss below. Similarly, activation of ALP-6 with zinc chloride also led to improved porosity of 1585, 1395, and 1057 m^2 g^{-1} for ALPDCZ500, ALPDCZ600, and ALPDCZ700, respectively. It seems that activation by $ZnCl_2$ has the most pronounced effect at 500 °C while increasing the activation temperature to 600 and 700 °C has negative impact on porosity. The mechanism of activation by $ZnCl_2$ differs from that of KOH. While the latter is a strong base, the former is a Lewis acid. In general, KOH activation mechanism is governed by the evolution of CO_x or C_xH_y gaseous species because of oxidative environment. It has been shown that for biomass precursors the $ZnCl_2$ activation is mainly dictated by dehydration upon increasing the temperature.[31] The $ZnCl_2$ reacts with the precursor after initial dehydration and inhibits further pore generation. As a result, slight degradation of textural properties for carbons activated at temperatures above 500 °C can be realized.[32] Olivares-Marín et al. performed a comprehensive study on the $ZnCl_2$ activation parameters (temperature and impregnation ratio) effect on textural properties of prepared carbons using Chery stone as a precursor. In a similar trend to our results, they noticed that among five carbons obtained by activation between 400 and 800 °C, the one prepared at 500 °C presented the highest surface area and micropore volume.[33]

Pore size distribution (PSD) of ALP-6 and its derived carbons were thoroughly investigated by N_2 (77 K) isotherms and quenched solid density functional theory (QSDFT) model which is widely employed for carbons with heterogeneous pore walls.[34] Moreover, CO_2 isotherms (273 K) and nonlocal density functional theory (NLDFT) model were employed to assess the distribution of fine micropores where nitrogen molecules diffusion is limited by extremely slow and time-consuming kinetic. In other words, higher kinetic energy of the CO_2 molecules at 273 K enables them to penetrate and probe narrower pores faster than N_2 and Ar molecules do at cryogenic temperatures. That is to say, the CO_2 isotherm presents more reliable data for distribution of pores below 0.7, while N_2 is more beneficial to evaluate the distribution of larger micropores, mesopores and any possible macropores. Consequently, the overall PSD spectra are achieved by information gathered from both N_2 and CO_2 isotherms and results are depicted in Figure S2. In a similar manner to N_2 isotherms, PSD curves for each class of ALP-6 derived carbons together with the ALP-6 parent precursor are stacked and demonstrated in Figures 1D–F. The pore size distribution of ALPDCDs is predominantly centered around 5 Å in contrast to the randomly distributed pores of ALP-6 all across the micropore size range (<2 nm). The PSD curves of KOH activated carbons (Figure 1E) indicate that their porosity is made of mostly micropores. The pore size of low temperature activated carbon, ALPDCK500, centers around 5 and 9 Å. Increasing the activation temperature to 600 and 700 °C not only shifts the dominant peaks to slightly higher values, but also adds a small fraction of narrow mesoporosity which distributed around 23–24 Å to the system. The pores of $ZnCl_2$ activated carbons were also realized to distribute around 5 and 9 Å (Figure 1F). A slight reduction in dominant pore size as well as appearance of narrow mesopores around 22 Å were observed upon increasing the activation temperature from 500 to 700 °C.

The pore volume of microporous carbons was studied in detail due to its significance in gas adsorption properties. Accordingly, the total pore volume (V_{Tot}, at P/P_0 = 0.95), the micropore volume (V_{Mic}, calculated by DFT and *t*-plot methods), the ratio of micro to total pore volume (V_{Mic}/V_{Tot}, as a degree of microporosity), and the volume of ultramicropores (V_0, pores below 7 Å) are calculated and summarized in Table 1. The total pore volume of merely carbonized samples decreases with respect to that of ALP-6. However, micropore volume, ultramicropore volume and percentage of microporosity increase at higher carbonization temperatures and reach to the highest values of 0.20 cm^3 g^{-1}, 0.15 cm^3 g^{-1} and 69% for ALPDCD800, respectively. Among KOH-activated carbons, the ALPDCK500 exhibits the lowest total pore volume (0.37 cm^3 g^{-1}) which is lower than that of ALP-6 (0.50 cm^3 g^{-1}). The ALPDCK700 exhibits the highest total and micropore volume of 1.26 cm^3 g^{-1} and 0.90 cm^3 g^{-1}, respectively, among all studied carbons. Importantly, ALPDCK600 possesses the highest volume of ultramicropores

DOI: 10.1021/acsami.6b00567
ACS Appl. Mater. Interfaces 2016, 8, 8491–8501

(0.35 cm^3 g^{-1}), which benefits small gas adsorption performance. The degree of microporosity dropped from 84 to 71% by increasing the activation temperature from 500 to 700 °C due to mesopore formation. Activation by $ZnCl_2$ led to enhancement in all types of pore volumes compared to ALP-6. As discussed above for surface area studies, the most effective activation mechanism at 500 °C results in the highest values for total, micro and ultramicro pore volume up to 0.71, 0.54, and 0.26 cm^3 g^{-1}, respectively. However, unlike KOH-activation the lack of effective pore formation mechanism for $ZnCl_2$ activation at elevated temperatures (600 and 700 °C) results in narrower pores. Therefore, the microporosity level shows slight improvement up to 80 and 82% for ALPDCZ600 and ALPDCZ700, respectively.

Microstructure and Composition Study. The SEM images of ALP-6 together with one representative sample of each series of carbons (synthesized at 600 °C) are presented in Figure 2 for comparison. The ALP-6 precursor displays a spherical morphology. The direct carbonized samples retain the original spherical shape with slight shrinkage in size compared to parent ALP-6. The $ZnCl_2$ activated carbons display a somewhat diverse microstructure. The most effective activation at 500 °C leads to destruction of the majority of the primary spheres existing in ALP-6 and converts them to smaller and more irregular-shaped phases. Interestingly, activation at 600 and 700 °C seems to be more effective in maintaining the original spherical morphology as ALPDCZ700 is composed of just spherical morphology with reduced particle size (Figures S3D–F). In contrast to the ALPDCD and ALPDCZ series, a dramatic morphological change was observed for KOH activated carbons. The activation by KOH results in total destruction of the original spherical morphology and the formation of massive irregular-shaped structures at all temperatures (Figures S3G–I). The noticeable morphological difference between $ZnCl_2$ and KOH activated carbons is due to their different activation mechanisms. The dehydration effect of $ZnCl_2$ occurs through the elimination of hydrogen and oxygen and as such the volatilization of the main carbon structure is less pronounced. Thus, the microstructure of parent precursor is mainly preserved in newly formed carbons. This observation is consistent with preserved spherical morphology of carbons derived by $ZnCl_2$ activation of poly divinylbenzene and polyfuran.[35,36] On the contrary, KOH activation takes place by evolution of volatile species (CO_2 and K_2O) and their reaction with carbon frameworks. It can be concluded that the new microstructure forms by simultaneous collapse and rearrangement of carbon framework upon heat treatment.

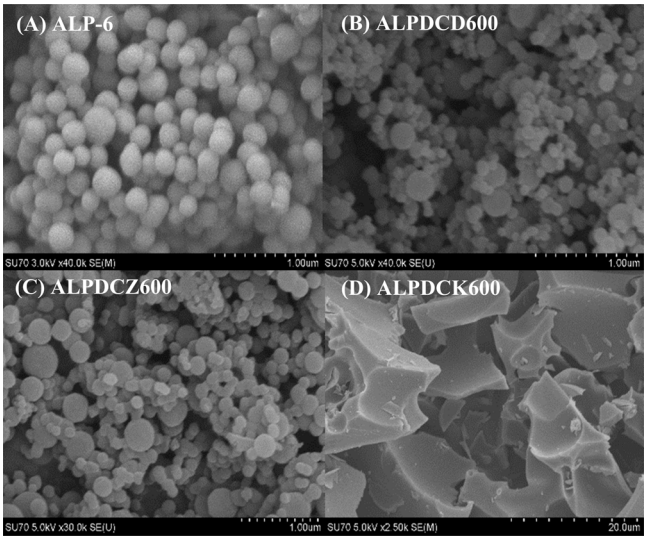

Figure 2. Scanning electron microscopy (SEM) images of (A) ALP-6, (B) ALPDCD600, (C) ALPDCK600, and (D) ALPDCZ600.

The chemical composition was evaluated by elemental analysis (EA). The CHN elemental composition (carbon, hydrogen, and nitrogen wt %), as well as the remaining ash content (wt %), of the studied carbons and parent polymer are summarized in Table 2. It is clear that both carbonization and activation led to diminution of nitrogen level with respect to that of ALP-6. The results showed that the nitrogen content in the ALPDCD and ALPDCK classes of carbons decreases by increasing the temperature whereas in the ALPDCZ series it slightly increases. The latter can be justified by the optimum $ZnCl_2$ activation at 500 °C as explained above. Three samples of ALPDCD600, ALPDCK500, and ALPDCZ700 retained the highest nitrogen level of 14.3, 12.1, and 13.7 wt %, respectively.

To study the oxygen and nitrogen species on the pore walls of ALPDCs, X-ray photoelectron spectroscopy (XPS) was performed. Survey spectra of all ALP-derived carbons, as well as ALP-6, distinctly feature three dominant peaks centered at 285.1, 399.9, and 532.7 eV corresponding to the presence of C 1s, N 1s, and O 1s, respectively (Figure S4). The absence of any other peaks in the full survey pattern clearly confirms the removal of metal traces during the acid washing process. The surface concentration of C, N and O are calculated from the

Table 2. Elemental Analysis and XPS Data for ALP-6 Derived Carbons and ALP-6

	CHN elemental analysis					XPS		
sample	C (wt %)	H (wt %)	N (wt %)	O[a] (wt %)	ash (wt %)	C (wt %)	N (wt %)	O (wt %)
ALP-6	69.5	4.2	14.7	11.6		76.7	12.5	10.8
ALPDCD600	78.7	2.7	14.3	3.8	0.5	83.5	11.8	4.7
ALPDCD700	80.3	1.7	12.6	4.2	1.2	84.4	9.4	6.2
ALPDCD800	80.0	1.0	8.5	8	2.5	84.6	7.4	8.0
ALPDCK500	61.5	2.3	12.1	19.6	4.5	72.3	9.8	17.9
ALPDCK600	68.7	1.6	9.3	18.5	1.9	74.3	8.5	17.2
ALPDCK700	73.2	1.0	4.7	19.2	1.9	79.0	4.9	16.1
ALPDCZ500	60.0	1.9	11.1	6.8	20.2	77.3	11.2	11.6
ALPDCZ600	71.7	1.7	12.6	9.7	4.3	79.0	10.8	10.2
ALPDCZ700	71.4	1.4	13.7	11	2.5	77.4	11.4	11.2

[a]Calculated by difference.

DOI: 10.1021/acsami.6b00567
ACS Appl. Mater. Interfaces 2016, 8, 8491–8501

corresponding peak areas of XPS spectra and results are summarized in Table 2. The percentages of carbon and nitrogen obtained by XPS are in agreement with values tested by elemental analysis. It should be taken into account that elemental analysis is carried out in the bulk of carbon material but XPS is a surface sensitive method and values for C, N and O content usually are gathered from the surface of samples. This reveals that the amounts of the surface nitrogen groups are slightly lower than the ones in the bulk materials. In contrast, the relatively higher amounts of carbon and oxygen reported by XPS can be ascribed to the possible adsorption of hydrocarbon contaminant[37] and moisture[38] on the surface during sample preparation. Moreover, the consistent results of XPS and EA reflects the uniform distribution of heteroatoms into the porous carbon framework. The nature of oxygen and nitrogen functionalities was further investigated by deconvolution of their 1s core level spectra. In general, four nitrogen species as N-6 (pyridinic), N-5 (pyrrolic and/or pyridonic), N-Q (quaternary), and N-X (oxidized), as well as three different components of oxygen groups as O-I (quinone), O-II (phenol or ether), and O-III (carboxylic groups or water) are mostly recognizable in porous carbons.[39,40] A schematic representation of all possible nitrogen and oxygen species for a typical porous carbons and ALP-6 network along with their binding energy has been depicted in Figure S5. High resolution deconvoluted N 1s and O 1s spectra of the ALP-6 derived carbons and the ALP-6 are depicted in Figures S6 and S7, respectively. Clearly, two different types of nitrogen (amine and azo) can be distinguished by the molecular formula of ALP-6, which are not correlated to any four species found in N-functionalized carbons. Surprisingly, after deconvolution and peak fitting just one single peak at 399.8 eV was recognized (denoted as N-A, hereafter). Interestingly, we found that Amine and Azo nitrogen groups have almost identical N 1s binding energies which explains their overlapping.[41] It is expected that pristine N-A nitrogen species evolve to N-5/N-6/N-Q/N-X surface groups in the course of heat treatment and activation. Consequently, the ALPDCD class possess all four types of nitrogen and three oxygen surface groups. By contrast, the quaternary nitrogen type (N-Q) is absent in ALPDCKs and ALPDCZs while the pyrrolic/pyridonic nitrogen (N-5) is found to be dominant. Notably, the chemical activation awards higher amounts of oxygen surface group to the resultant carbons due to the oxidative and dehydrating effects of KOH and $ZnCl_2$, respectively. It also has been observed that nitrogen functional groups oxidize easily[32,42] which further supports the presence of N-X type nitrogen in all studied carbons. For the sake of comparison, nitrogen species of one representative sample of each class of carbons (ALPDCD600, ALPDCK600, ALPDCZ600) and ALP-6 are also shown in Figure 3 together.

CO_2 and CH_4 Capture Performance. Motivated by the large portion of microporosity and high level of basic heteroatoms (O and N) generated during carbonization/activation process, the CO_2 capture performance of ALPDCs were explored by collecting their isotherms up to 1 bar. A comparative analysis of CO_2 adsorption isotherms measured at 273 and 298 K for each class of ALP-6 derived carbons as well as ALP-6 is illustrated in Figures 4 A-F. As shown in Figure 4 A, at 273 K the low temperature carbonized samples (ALPDCD600 and ALPDC700) exhibit slightly lower CO_2 uptake at 1 bar compared to ALP-6 while ALPDCD800 features slight improvement in final uptake. As evidenced by Figure 4D, at 298 K the ALPDCD800 features noticeable

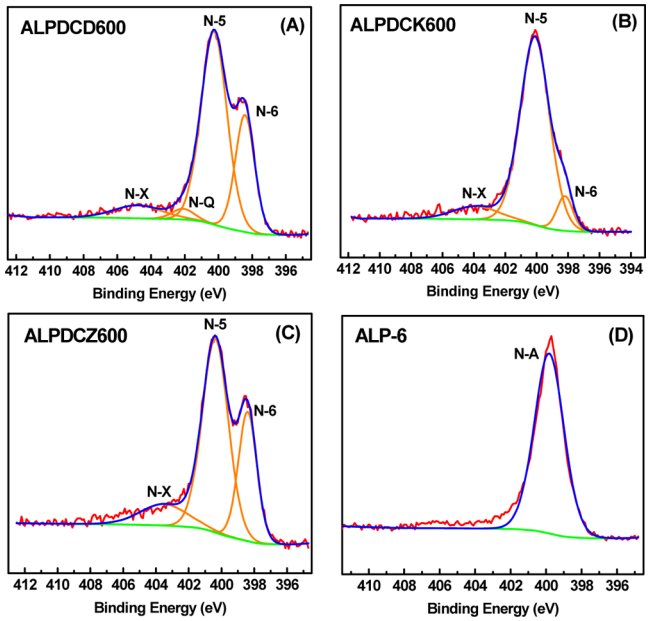

Figure 3. High-resolution deconvoluted N 1s spectra for (A) ALPDCD600, (B) ALPDCK600, (C) ALPDCZ600, and (D) ALP-6.

improvement in uptake while ALPDCD600 and ALPDCD700 show almost similar uptake to the parent polymer. All three KOH-activated carbons show substantial enhancement in CO_2 adsorption due to the generation of micropores and evolution of basic nitrogen and oxygen surface groups throughout the studied pressure range. However, the ALPDCK500 with the lowest volume of micropore and the highest level of total heteroatoms presents a lower rate of increase in uptake at pressures higher than 0.4 bar. By contrast, the ALPDCK600 and ALPDCK700 demonstrate a steady rise in CO_2 uptake for the entire pressure range thanks to the larger micropore volume despite their lower heteroatom content (Figure 4B and Figure 4E). The comparison of three KOH-activated carbons implies that CO_2 capture capacity at a certain pressure is a function of basic functionalities and microporosity. While the role of pore heterogeneity is more prominent at lower relative pressures, the structural properties has a more pronounced effect on adsorption capacity at 1 bar and higher pressures. Due to the importance of narrow micropores in CO_2 adsorption, the volume of certain ultramicropores are calculated and tabulated in Table S1. At 1 bar the ALPDCK600 features the highest CO_2 uptake values of 8.3 and 5.2 mmol g^{-1} at 273 and 298 K, respectively, which are comparable to the highest heteroatom doped microporous carbon reported to date.[14,17,21,26,43,44] Similarly, three $ZnCl_2$-activated carbons show superior adsorption capacity at 1 bar with respect to ALP-6 (Figure 4C and Figure 4F). The highest CO_2 uptakes, 6.2 and 3.9 mmol g^{-1} were achieved on ALPDCZ500 at 273 and 298 K, respectively. In general, the ALPDCZs show slightly lower CO_2 capture capacity compared to their KOH-activated counterparts. This can be justified by different mechanisms of gasification and dehydration for KOH and $ZnCl_2$, respectively. The dehydration process by $ZnCl_2$ takes place by combining oxygen and hydrogen upon the decomposition of oxygen containing functional groups in the precursors. This leads to lower amount of heteroatoms (combination of oxygen and nitrogen) in ALPDCZs with respect to ALPDCKs. Moreover, the KOH activation is well-known for introducing ultrafine

DOI: 10.1021/acsami.6b00567
ACS Appl. Mater. Interfaces 2016, 8, 8491−8501

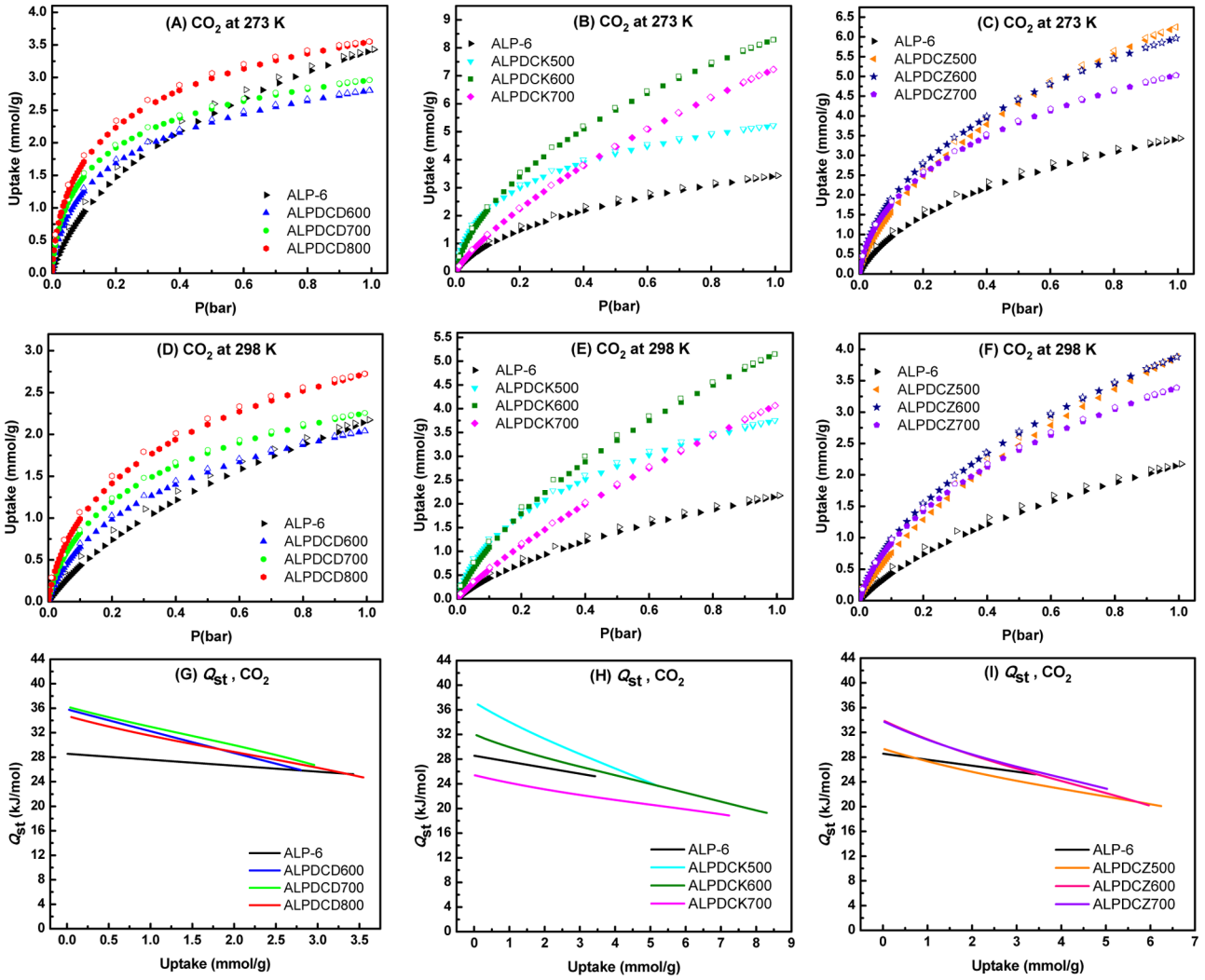

Figure 4. CO_2 adsorption isotherms at (A–C) 273 and (D–F) 298 K and (G–I) CO_2 isosteric heats of adsorption for ALP-6 derived carbons and ALP-6.

Table 3. Gas Uptakes, Isosteric Heats of Adsorption, and Selectivity (CO_2/N_2 and CO_2/CH_4) for ALP-6 Derived Carbons and ALP-6[a]

	CO_2					CH_4			selectivity	
	0.15 bar		1.0 bar			1.0 bar				
sample	273 K	298 K	273 K	298 K	Q_{st}	273 K	298 K	Q_{st}	CO_2/N_2	CO_2/CH_4
ALP-6	1.2	0.6	3.4	2.2	28.6	1.0	0.60	19.0	45 (48)	10 (7)
ALPDCD600	1.5	0.8	2.8	2.0	35.8	1.2	0.7	25.2	89 (54)	12 (8)
ALPDCD700	1.7	1.0	3.0	2.3	36.3	1.4	1.0	24.8	79 (54)	9 (8)
ALPDCD800	2.0	1.2	3.5	2.7	34.7	1.7	1.2	24.3	64 (42)	9 (7)
ALPDCK500	2.7	1.5	5.2	3.8	37.2	1.7	1.1	22.5	115 (62)	18 (11)
ALPDCK600	2.9	1.5	8.3	5.2	32.0	2.4	1.4	20.3	62 (36)	13 (8)
ALPDCK700	1.8	0.9	7.2	4.1	25.4	2.4	1.5	18.2	22 (14)	5 (4)
ALPDCZ500	2.1	1.0	6.2	3.9	29.4	1.9	1.1	21.1	47 (27)	10 (6)
ALPDCZ600	2.4	1.3	6.0	3.9	34.0	2.0	1.2	21.2	70 (41)	12 (9)
ALPDCZ700	2.2	1.2	5.0	3.4	33.8	1.8	1.1	22.2	74 (45)	13 (9)

[a]Gas uptake in mmol g^{-1}, isosteric heats of adsorption (Q_{st}) in kJ mol^{-1}, and selectivity mol mol^{-1} at 273 K (298 K)

pores into the system.[36] The role of basic heteroatoms and narrow micropores will be discussed in detail in the following paragraphs.

To investigate the binding affinity of ALP-derived carbons for CO_2, isosteric heats of adsorption (Q_{st}) were calculated by the virial method using CO_2 adsorption isotherms collected at 273 and 298 K.[45] The plots of Q_{st} (kJ mol^{-1}) as a function of CO_2 uptake (mmol g^{-1}) are shown in Figures 4G–I and Q_{st} values at zero coverage are provided in Table 3. The polymer precursor features the intermediate isosteric heat of adsorption

DOI: 10.1021/acsami.6b00567
ACS Appl. Mater. Interfaces 2016, 8, 8491–8501

of 28.5 kJ mol^{-1} at zero loading. After direct carbonization, the Q_{st} values significantly increased to 34.7−36.3 kJ mol^{-1}. This dramatic improvement in Q_{st} can be explained by the shrinkage of the initial microporosity in ALP-6 and providing much smaller pores, which are more beneficial for interaction with CO_2 molecules. The Q_{st} values of 37.2, 32.0, and 25.4 kJ mol^{-1} were obtained for samples which are KOH activated at 500, 600, and 700 °C, respectively. The very high Q_{st} for ALPDCK500 at low CO_2 coverage takes place due to a cooperative effect of enhanced adsorbate−adsorbent interaction on ultrafine micropores and/or surface interaction between CO_2 and N/O basic heteroatoms.[46] Considering the almost identical volume of ultrafine pores for ALPDCK500 and ALPDCK600 (or even higher for ALPDCK600 for PV> 0.5 nm, Table S1), the effective role of higher percentage of total heteroatoms in ALPDCK500 becomes more pronounced. The decreasing trend with relatively large steps in Q_{st} of ALPDCKs can be rationalized by noticeable loss of the heteroatom content and pore widening upon increasing the activation temperature. Considering the fact that $ZnCl_2$-activated carbons possess nearly a similar amount of heteroatoms, their Q_{st} values are just controlled by their different volume of ultrafine pores. Both ALPDCZ600 and ALPDCZ700 samples show the highest Q_{st} values (34 kJ mol^{-1}) evidently because of higher volume of ultrafine pores.

To have a more accurate assessment about the merit of our ALP-6 derived carbons as sorbents for practical CO_2 capture and separation, their CO_2 adsorption behavior should be studied at the low pressure region of their isotherms which corresponds to CO_2 pressure in flue gas condition (3−15% by volume).[47] Thus, low pressure uptake isotherms of each class of ALP-6 derived carbons as well as ALP-6 precursor at 273 and 298 K are presented in Figure S8. All studied carbon materials show improved CO_2 capture at 0.15 bar, which further highlights the effectiveness of our carbonization and activation strategies. Namely, ALPDCD800, ALPDCK500 and ALPDCZ600 show substantial CO_2 uptake of 1.2, 1.5, and 1.3 mmol g^{-1} at 298 K/0.15 bar, respectively, featuring a minimum of two times improvement compared to 0.6 mmol g^{-1} value for ALP-6 precursor (Figure 5). The 1.5 mmol CO_2 capture per gram of the ALPDCK500 lies among the highest values and competes with the best performing porous carbons reported to date under similar conditions. It is comparable to

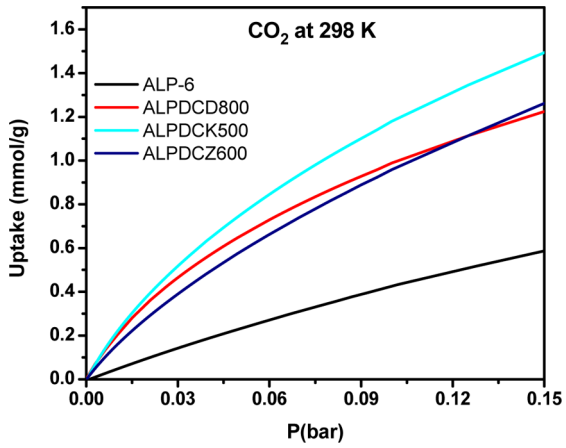

Figure 5. Low-pressure CO_2 uptake comparison of selected ALPDCs and ALP-6 at 298 K.

carbonized PAF with extra framework (1.35 mmol g^{-1}),[48] direct carbonized ZIF-8 with extra framework (1.53 mmol g^{-1}),[18] N-doped microporous carbons derived from direct carbonization of K^+ exchanged meta-aminophenol−formaldehyde resin (1.67 mmol g^{-1}),[49] carbons prepared by mechanochemical activation of sawdust at 600 °C (2 mmol g^{-1})[50] and KOH-activation of benzimidazole-linked polymers (2.1 mmol g^{-1}).[17] This result is consistent with the Q_{st} observations and the fact that enhanced CO_2 uptake at low pressure is mostly governed by the synergistic effect of high fraction of ultramicropores (V_0 in Table 1) and basic heteroatoms on the pore walls. The former provide stronger adsorption potential for confinement of the CO_2 molecule (kinetic size 3.3 Å)[51] while the latter introduce high charge density to the carbon network and favor binding to polarizable acidic CO_2 through hydrogen bonding and/or Lewis acid−base interactions.[52−54] Numerous theoretical research works have shown that the introduction of accessible nitrogen-donor groups into the internal walls of porous materials can dramatically improve the selective adsorption of CO_2.[55−57] The two pyridinic and pyrrolic functionalities are located at the edge of carbon framework (Figure S5B) and therefore exhibit high affinity toward CO_2 molecules. Although both pyridinic and pyrrolic types of nitrogen have a lone pair of electrons, the pyridinic species offers higher basicity because of its more accessible electron.[58] This makes pyridinic nitrogen advantageous for effective binding to the electron deficient center of the carbon atom at low CO_2 coverage. Additionally, the hydrogen present on pyrrolic/pyridonic groups contributes more positively to CO_2 capture by inducing NH···O hydrogen bonding. Despite the comprehensive literature study on the effectiveness of nitrogen basic groups on the CO_2 separation (or CO_2 capture at low partial pressure) of various porous solids, the role of oxygen functionalities has been largely underestimated if not ignored. More specifically, when an oxygen rich precursor (such as biomass) and/or an oxidizing activating agent (such as KOH) is used, considerable amount of oxygen will be doped into the framework of carbon.[11,14] Results from theoretical studies confirm that oxygen containing functional groups such as ether, hydroxyl and carbonyl have significant impact on CO_2 selective adsorption of porous polymers and carbons.[59−61] In a similar manner to nitrogen functional groups, the oxygen sites facilitate the dipole-quadruple interaction and/or hydrogen bonding with CO_2 molecules

To further highlight the effect of basic heteroatoms on the uptake at low CO_2 partial pressure condition, three KOH-activated carbons were selected due to their high heteroatoms content and diverse textural properties. The comparison of low pressure regime of ALPDCKs isotherms at a certain temperature shows that ALPDCK500 with the highest percentage of total heteroatom (30 wt % N and O) exhibits higher uptake than the other two samples. The fact that ALPDCK600 and ALPDCK700 with higher amount of micropore and ultramicropore volume but lower amount of total heteroatoms featured inferior uptake further validates the significant contribution of heteroatoms. Additionally the CO_2 adsorption isotherms of ALPDCKs at elevated temperatures of 323 and 348 K were collected (Figure S9). The results confirmed that these samples are still able to capture CO_2 especially at low pressures. This observation further supports the key role of heteroatoms in CO_2 binding because at elevated temperatures

DOI: 10.1021/acsami.6b00567
ACS Appl. Mater. Interfaces 2016, 8, 8491−8501

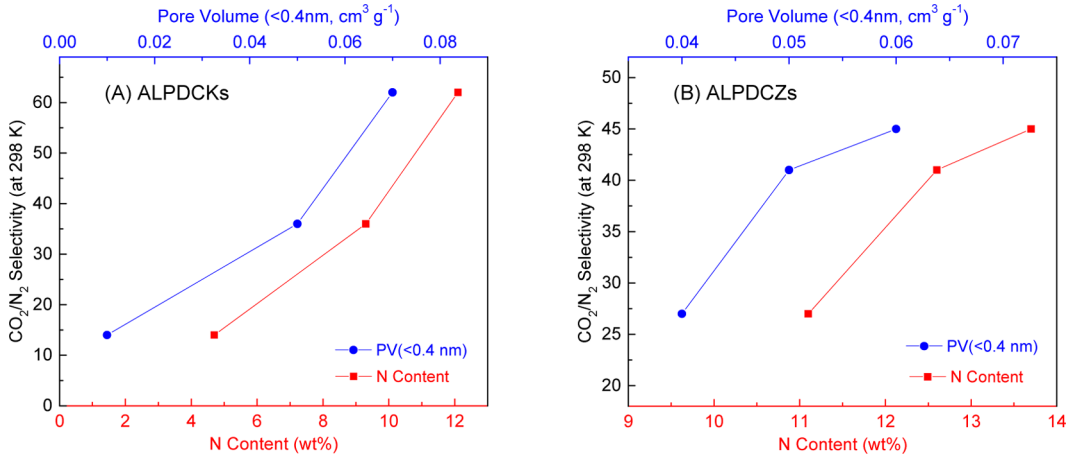

Figure 6. Correlation between CO_2/N_2 selectivity (at 298 K) and nitrogen content (red) and the volume of ultrafine micropores (blue) for (A) ALPDCKs and (B) ALPDCZs.

the high thermal motion of CO_2 molecules makes physical adsorption by weak adsorbate−adsorbent interaction less likely.

We also investigated the methane adsorption at 273 and 298 K and low pressure for gas separation studies. The results are displayed in Figures S10 (A−F) and summarized in Table 3. All ALP-6 derived carbons exhibit superior methane adsorption performance for the entire pressure range in comparison with the polymer precursor. The role of basic heteroatoms can be ruled out because of the very low polarizability of methane (26×10^{-25} cm^3).[62] Therefore, the improvement of methane uptake can be solely correlated with modified textural properties after carbonization/activation. A closer observation of methane isotherms for three classes of carbons reveals that direct carbonized samples show higher uptake at low pressures (up to 0.2 bar) while ALPDCZ and ALPDCK series exhibit greater uptake at higher pressures (0.2−1 bar). Moreover, none of the studied carbons reaches to saturation uptake at 1 bar suggesting a higher CH_4 capacity could be achieved by increasing the pressure above 1 bar. From the last two statements, it can be concluded that methane uptake at very low pressures is governed by narrow pores. As the pore size increases, the higher amount of methane will also be adsorbed at higher pressure. The measured methane heats of adsorption (Figures S10G−I and Table 3) further validate previously explained adsorption trend where direct carbonized samples presented extremely high heat of adsorption ranging between 24.3 and 25.3 kJ mol^{-1} at zero coverage. This high amount of energy compared to 19 kJ mol^{-1} for ALP-6 can be justified by increasing the number of very small pores generated by shrinkage of the primary porosity.

Selective Adsorption of CO_2 over N_2 and CH_4. To this end, we showed that transformation of azo-linked polymer to heteroatom doped carbons resulted in improvement of CO_2 adsorption capacity. However, for practical application such as separation of CO_2 from flue gas, landfill gas and natural gas, selective adsorption of CO_2 over other gases in the mixture (mainly N_2 and CH_4) also needs to be fulfilled along with high uptake value. Excellent uptake of studied carbons at low pressure, high amounts of basic heteroatoms and abundance of microporosity would be expected to afford high selectivity of CO_2 over N_2 and CH_4. The selectivity was probed using the initial slope ratios measured according to Henry's law constant for single component adsorption components at low pressure coverage. The N_2 isotherms at 273 and 298 K were also collected and presented together with previously measured CO_2 and CH_4 isotherms in Figures S11 and S12. It is clearly observed that the amount of CO_2 adsorbed is much higher than for CH_4 and N_2 in all tested pressure range. The initial slopes calculation for ALP-6 derived carbons at 273 and 298 K are shown in Figures S13 and S14 and selectivity values of CO_2/N_2 and CO_2/CH_4 are provided in Table 3. The analogous trend of selectivity results to Q_{st} values at low loading indicates the importance of heteroatoms and ultramicropores. It should be emphasized that since N_2 and CH_4 are not able to interact with basic functionalities through hydrogen bond and/or dipole−quadrupole interactions, it is expected that any decrease in heteroatoms content reduce the CO_2 selectivity values. In other words, CO_2-philic sites (N and O) are considered as key parameters for the selective CO_2 adsorption over N_2 and CH_4.[63] Thus, it is believed that basic functional groups on the pore walls of carbons play a more important role than pore size in selectivity. As in direct carbonized samples, the ALPDCD600 sample shows the highest CO_2/N_2 and CO_2/CH_4 of 89 and 12 at 273 K, respectively. Further increase in carbonization temperature resulted in elimination of more basic surface groups and the decline of selectivity values. The ALPDCK500 carbon features remarkable CO_2 selectivity values of 118 (over N_2) and 18 (over CH_4) at 273 K, mainly due to collaborating effect of narrow micropores and high level of heteroatoms (~30 wt % total). Considering the similar amount of total heteroatom in all three $ZnCl_2$-activated carbons, the highest selectivity was observed for ALPDCZ700, which has smaller pores. These values reach up to 74 and 13 for CO_2/N_2 and CO_2/CH_4 at 273 K, respectively. The correlation between CO_2/N_2 selectivity at 298 K and nitrogen percentage and the volume of ultrafine pores (below 0.4 nm) has been demonstrated in Figure 6.

CONCLUSION

Three different strategies based on direct carbonization and $ZnCl_2$ and KOH activation were applied to transform an azo-linked polymer (ALP-6) into microporous heteroatom-doped carbons. By adjusting the activation temperature, a diverse range of textural properties such as surface area, pore volume and microporosity was achieved. The resultant carbons contained high amount of Lewis basic functionalities (nitrogen and oxygen), which vary with activation methods and pyrolysis temperatures. At 298 K, the carbon materials show high CO_2

DOI: 10.1021/acsami.6b00567
ACS Appl. Mater. Interfaces 2016, 8, 8491−8501

adsorption capacity with values as high as 5.2 mmol g^{-1} (1 bar) and 1.5 mmol g^{-1} (0.15 bar). This high CO_2 uptake capacity is attributed to the combined effect of high levels of narrow micropores and a high density of oxygen and nitrogen basic functionalities on the pore walls. Moreover, the prepared carbons discriminate CO_2 from other gases with relatively similar sizes such as CH_4 and N_2 to attain high selectivity levels of 115 for CO_2/N_2 and 18 for CO_2/CH_4 at 273 K. Although the reported microporous carbons exhibit high and selective CO_2 capture, challenges such as scalability and cost need to be addressed for their consideration in practical applications.

■ ASSOCIATED CONTENT

Supporting Information

The Supporting Information is available free of charge on the ACS Publications website at DOI: 10.1021/acsami.6b00567.

Synthesis and characterization of porous carbons and their gas uptake and selectivity studies (PDF)

■ AUTHOR INFORMATION

Corresponding Author

*E-mail: helkaderi@vcu.edu. Fax: +1 804 828 8599. Tel: +1 04 828 7505.

Notes

The authors declare no competing financial interest.

■ ACKNOWLEDGMENTS

This work was supported by the U.S. Department of Energy, Office of Basic Energy Sciences, Division of Materials Sciences and Engineering under award number (DE-SC0002576). This work is supported in part by CIT CRCF.

■ REFERENCES

(1) Kennedy, C.; Steinberger, J.; Gasson, B.; Hansen, Y.; Hillman, T.; Havránek, M.; Pataki, D.; Phdungsilp, A.; Ramaswami, A.; Mendez, G. V. Greenhouse Gas Emissions from Global Cities. *Environ. Sci. Technol.* **2009**, *43*, 7297−7302.

(2) Scott, V.; Gilfillan, S.; Markusson, N.; Chalmers, H.; Haszeldine, R. S. Last Chance for Carbon Capture and Storage. *Nat. Clim. Change* **2013**, *3*, 105−111.

(3) Haszeldine, R. S. Carbon Capture and Storage: How Green Can Black Be? *Science* **2009**, *325*, 1647−1652.

(4) Markewitz, P.; Kuckshinrichs, W.; Leitner, W.; Linssen, J.; Zapp, P.; Bongartz, R.; Schreiber, A.; Muller, T. E. Worldwide Innovations in the Development of Carbon Capture Technologies and the Utilization of CO_2. *Energy Environ. Sci.* **2012**, *5*, 7281−7305.

(5) D'Alessandro, D. M.; Smit, B.; Long, J. R. Carbon Dioxide Capture: Prospects for New Materials. *Angew. Chem., Int. Ed.* **2010**, *49*, 6058−6082.

(6) Rochelle, G. T. Amine Scrubbing for CO_2 Capture. *Science* **2009**, *325*, 1652−1654.

(7) Wang, J.; Huang, L.; Yang, R.; Zhang, Z.; Wu, J.; Gao, Y.; Wang, Q.; O'Hare, D.; Zhong, Z. Recent Advances in Solid Sorbents for CO_2 Capture and New Development Trends. *Energy Environ. Sci.* **2014**, *7*, 3478−3518.

(8) Lu, A.-H.; Hao, G.-P. Porous Materials for Carbon Dioxide Capture. *Annu. Rep. Prog. Chem., Sect. A: Inorg. Chem.* **2013**, *109*, 484−503.

(9) Bae, Y.-S.; Snurr, R. Q. Development and Evaluation of Porous Materials for Carbon Dioxide Separation and Capture. *Angew. Chem., Int. Ed.* **2011**, *50*, 11586−11596.

(10) Wang, J.; Kaskel, S. KOH Activation of Carbon-Based Materials for Energy Storage. *J. Mater. Chem.* **2012**, *22*, 23710−23725.

(11) Sevilla, M.; Valle-Vigón, P.; Fuertes, A. B. N-Doped Polypyrrole-Based Porous Carbons for CO_2 Capture. *Adv. Funct. Mater.* **2011**, *21*, 2781−2787.

(12) Xia, Y.; Mokaya, R.; Walker, G. S.; Zhu, Y. Superior CO_2 Adsorption Capacity on N-Doped, High-Surface-Area, Microporous Carbons Templated from Zeolite. *Adv. Energy Mater.* **2011**, *1*, 678−683.

(13) Jalilov, A. S.; Ruan, G.; Hwang, C.-C.; Schipper, D. E.; Tour, J. J.; Li, Y.; Fei, H.; Samuel, E. L. G.; Tour, J. M. Asphalt-Derived High Surface Area Activated Porous Carbons for Carbon Dioxide Capture. *ACS Appl. Mater. Interfaces* **2015**, *7*, 1376−1382.

(14) Sevilla, M.; Fuertes, A. B. Sustainable Porous Carbons with a Superior Performance for CO_2 Capture. *Energy Environ. Sci.* **2011**, *4*, 1765−1771.

(15) Wickramaratne, N. P.; Jaroniec, M. Activated Carbon Spheres for CO_2 Adsorption. *ACS Appl. Mater. Interfaces* **2013**, *5*, 1849−1855.

(16) Nandi, M.; Okada, K.; Dutta, A.; Bhaumik, A.; Maruyama, J.; Derks, D.; Uyama, H. Unprecedented CO_2 Uptake over Highly Porous N-Doped Activated Carbon Monoliths Prepared by Physical Activation. *Chem. Commun.* **2012**, *48*, 10283−10285.

(17) Ashourirad, B.; Sekizkardes, A. K.; Altarawneh, S.; El-Kaderi, H. M. Exceptional Gas Adsorption Properties by Nitrogen-Doped Porous Carbons Derived from Benzimidazole-Linked Polymers. *Chem. Mater.* **2015**, *27*, 1349−1358.

(18) Aijaz, A.; Fujiwara, N.; Xu, Q. From Metal−Organic Framework to Nitrogen-Decorated Nanoporous Carbons: High CO_2 Uptake and Efficient Catalytic Oxygen Reduction. *J. Am. Chem. Soc.* **2014**, *136*, 6790−6793.

(19) Gadipelli, S.; Guo, Z. X. Tuning of ZIF-Derived Carbon with High Activity, Nitrogen Functionality, and Yield - A Case for Superior CO_2 Capture. *ChemSusChem* **2015**, *8*, 2123−2132.

(20) Wang, J.; Senkovska, I.; Oschatz, M.; Lohe, M. R.; Borchardt, L.; Heerwig, A.; Liu, Q.; Kaskel, S. Imine-Linked Polymer-Derived Nitrogen-Doped Microporous Carbons with Excellent CO_2 Capture Properties. *ACS Appl. Mater. Interfaces* **2013**, *5*, 3160−3167.

(21) Wang, J.; Senkovska, I.; Oschatz, M.; Lohe, M. R.; Borchardt, L.; Heerwig, A.; Liu, Q.; Kaskel, S. Highly Porous Nitrogen-Doped Polyimine-Based Carbons with Adjustable Microstructures for CO_2 Capture. *J. Mater. Chem. A* **2013**, *1*, 10951−10961.

(22) Yang, X.; Yu, M.; Zhao, Y.; Zhang, C.; Wang, X.; Jiang, J.-X. Remarkable Gas Adsorption by Carbonized Nitrogen-Rich Hypercrosslinked Porous Organic Polymers. *J. Mater. Chem. A* **2014**, *2*, 15139−15145.

(23) Wang, C.; Luo, H.; Jiang, D. E.; Li, H.; Dai, S. Carbon Dioxide Capture by Superbase-Derived Protic Ionic Liquids. *Angew. Chem., Int. Ed.* **2010**, *49*, 5978−5981.

(24) Zhang, S.; Dokko, K.; Watanabe, M. Carbon Materialization of Ionic Liquids: From Solvents to Materials. *Mater. Horiz.* **2015**, *2*, 168−197.

(25) Adeniran, B.; Masika, E.; Mokaya, R. A Family of Microporous Carbons Prepared via a Simple Metal Salt Carbonization Route with High Selectivity for Exceptional Gravimetric and Volumetric Post-Combustion CO_2 Capture. *J. Mater. Chem. A* **2014**, *2*, 14696−14710.

(26) Chen, G.; Wang, X.; Li, J.; Hou, W.; Zhou, Y.; Wang, J. Direct Carbonization of Cyanopyridinium Crystalline Dicationic Salts into Nitrogen-Enriched Ultra-Microporous Carbons toward Excellent CO_2 Adsorption. *ACS Appl. Mater. Interfaces* **2015**, *7*, 18508−18518.

(27) Zhu, H.; Yin, J.; Wang, X.; Wang, H.; Yang, X. Microorganism-Derived Heteroatom-Doped Carbon Materials for Oxygen Reduction and Supercapacitors. *Adv. Funct. Mater.* **2013**, *23*, 1305−1312.

(28) Fan, X.; Zhang, L.; Zhang, G.; Shu, Z.; Shi, J. Chitosan Derived Nitrogen-Doped Microporous Carbons for High Performance CO_2 Capture. *Carbon* **2013**, *61*, 423−430.

(29) Dutta, S.; Bhaumik, A.; Wu, K. C. W. Hierarchically Porous Carbon Derived from Polymers and Biomass: Effect of Interconnected Pores on Energy Applications. *Energy Environ. Sci.* **2014**, *7*, 3574−3592.

DOI: 10.1021/acsami.6b00567
ACS Appl. Mater. Interfaces 2016, 8, 8491−8501

(30) Arab, P.; Parrish, E.; Islamoglu, T.; El-Kaderi, H. M. Synthesis and Evaluation of Porous Azo-Linked Polymers for Carbon Dioxide Capture and Separation. *J. Mater. Chem. A* **2015**, *3*, 20586−20594.
(31) Caturla, F.; Molina-Sabio, M.; Rodríguez-Reinoso, F. Preparation of Activated Carbon by Chemical Activation with $ZnCl_2$. *Carbon* **1991**, *29*, 999−1007.
(32) Molina-Sabio, M.; Rodríguez-Reinoso, F. Role of Chemical Activation in the Development of Carbon Porosity. *Colloids Surf., A* **2004**, *241*, 15−25.
(33) Olivares-Marín, M.; Fernández-González, C.; Macías-García, A.; Gómez-Serrano, V. Preparation of Activated Carbon from Cherry Stones by Chemical Activation with $ZnCl_2$. *Appl. Surf. Sci.* **2006**, *252*, 5967−5971.
(34) Hu, X.; Radosz, M.; Cychosz, K. A.; Thommes, M. CO_2-Filling Capacity and Selectivity of Carbon Nanopores: Synthesis, Texture, and Pore-Size Distribution from Quenched-Solid Density Functional Theory (QSDFT). *Environ. Sci. Technol.* **2011**, *45*, 7068−7074.
(35) Zhu, Z.; Li, A.; Yan, L.; Liu, F.; Zhang, Q. Preparation and Characterization of Highly Mesoporous Spherical Activated Carbons from Divinylbenzene-Derived Polymer by $ZnCl_2$ Activation. *J. Colloid Interface Sci.* **2007**, *316*, 628−634.
(36) Wang, J.; Krishna, R.; Wu, X.; Sun, Y.; Deng, S. Polyfuran-Derived Microporous Carbons for Enhanced Adsorption of CO_2 and CH_4. *Langmuir* **2015**, *31*, 9845−9852.
(37) Smith, G. C. Evaluation of a Simple Correction for the Hydrocarbon Contamination Layer in Quantitative Surface Analysis by XPS. *J. Electron Spectrosc. Relat. Phenom.* **2005**, *148*, 21−28.
(38) Arab, P.; Verlander, A.; El-Kaderi, H. M. Synthesis of a Highly Porous Bis(Imino)Pyridine-Linked Polymer and Its Postsynthetic Modification with Inorganic Fluorinated Ions for Selective CO_2 Capture. *J. Phys. Chem. C* **2015**, *119*, 8174−8182.
(39) Pels, J. R.; Kapteijn, F.; Moulijn, J. A.; Zhu, Q.; Thomas, K. M. Evolution of Nitrogen Functionalities in Carbonaceous Materials During Pyrolysis. *Carbon* **1995**, *33*, 1641−1653.
(40) Hulicova-Jurcakova, D.; Seredych, M.; Lu, G. Q.; Bandosz, T. J. Combined Effect of Nitrogen- and Oxygen-Containing Functional Groups of Microporous Activated Carbon on its Electrochemical Performance in Supercapacitors. *Adv. Funct. Mater.* **2009**, *19*, 438−447.
(41) Tian, Z.; Dai, S.; Jiang, D.-e. Stability and Core-Level Signature of Nitrogen Dopants in Carbonaceous Materials. *Chem. Mater.* **2015**, *27*, 5775−5781.
(42) Rodríguez-Reinoso, F.; Molina-Sabio, M. Activated Carbons from Lignocellulosic Materials by Chemical and/or Physical Activation: An Overview. *Carbon* **1992**, *30*, 1111−1118.
(43) Wahby, A.; Ramos-Fernandez, J. M.; Martinez-Escandell, M.; Sepulveda-Escribano, A.; Silvestre-Albero, J.; Rodriguez-Reinoso, F. High-Surface-Area Carbon Molecular Sieves for Selective CO_2 Adsorption. *ChemSusChem* **2010**, *3*, 974−81.
(44) Wickramaratne, N. P.; Jaroniec, M. Importance of Small Micropores in CO_2 Capture by Phenolic Resin-Based Activated Carbon Spheres. *J. Mater. Chem. A* **2013**, *1*, 112−116.
(45) Czepirski, L.; JagieŁŁo, J. Virial-Type Thermal Equation of Gas-Solid Adsorption. *Chem. Eng. Sci.* **1989**, *44*, 797−801.
(46) Jin, Y.; Hawkins, S. C.; Huynh, C. P.; Su, S. Carbon Nanotube Modified Carbon Composite Monoliths as Superior Adsorbents for Carbon Dioxide Capture. *Energy Environ. Sci.* **2013**, *6*, 2591−2596.
(47) Lee, K. B.; Sircar, S. Removal and Recovery of Compressed CO_2 from Flue Gas by a Novel Thermal Swing Chemisorption Process. *AIChE J.* **2008**, *54*, 2293−2302.
(48) Zhang, Y.; Li, B.; Williams, K.; Gao, W.-Y.; Ma, S. A New Microporous Carbon Material Synthesized via Thermolysis of a Porous Aromatic Framework Embedded with an Extra Carbon Source for Low-Pressure CO_2 Uptake. *Chem. Commun.* **2013**, *49*, 10269−10271.
(49) Zhou, J.; Li, Z.; Xing, W.; Zhu, T.; Shen, H.; Zhuo, S. N-Doped Microporous Carbons Derived from Direct Carbonization of K^+ Exchanged Meta-Aminophenol-Formaldehyde Resin for Superior CO_2 Sorption. *Chem. Commun.* **2015**, *51*, 4591−4594.
(50) Balahmar, N.; Mitchell, A. C.; Mokaya, R. Generalized Mechanochemical Synthesis of Biomass-Derived Sustainable Carbons for High Performance CO_2 Storage. *Adv. Energy Mater.* **2015**, *5*, 1500867.
(51) Presser, V.; McDonough, J.; Yeon, S.-H.; Gogotsi, Y. Effect of Pore Size on Carbon Dioxide Sorption by Carbide Derived Carbon. *Energy Environ. Sci.* **2011**, *4*, 3059−3066.
(52) Hao, G. P.; Li, W. C.; Qian, D.; Lu, A. H. Rapid Synthesis of Nitrogen-Doped Porous Carbon Monolith for CO_2 Capture. *Adv. Mater.* **2010**, *22*, 853−7.
(53) Sekizkardes, A. K.; Altarawneh, S.; Kahveci, Z.; İslamoğlu, T.; El-Kaderi, H. M. Highly Selective CO_2 Capture by Triazine-Based Benzimidazole-Linked Polymers. *Macromolecules* **2014**, *47*, 8328−8334.
(54) Rabbani, M. G.; El-Kaderi, H. M. Template-Free Synthesis of a Highly Porous Benzimidazole-Linked Polymer for CO_2 Capture and H_2 Storage. *Chem. Mater.* **2011**, *23*, 1650−1653.
(55) Vogiatzis, K. D.; Mavrandonakis, A.; Klopper, W.; Froudakis, G. E. Ab Initio Study of the Interactions between CO_2 and N-Containing Organic Heterocycles. *ChemPhysChem* **2009**, *10*, 374−383.
(56) Vaidhyanathan, R.; Iremonger, S. S.; Shimizu, G. K. H.; Boyd, P. G.; Alavi, S.; Woo, T. K. Direct Observation and Quantification of CO_2 Binding within an Amine-Functionalized Nanoporous Solid. *Science* **2010**, *330*, 650−653.
(57) Vaidhyanathan, R.; Iremonger, S. S.; Dawson, K. W.; Shimizu, G. K. H. An Amine-Functionalized Metal Organic Framework for Preferential CO_2 adsorption at Low Pressures. *Chem. Commun.* **2009**, 5230−5232.
(58) Richter, F. P.; Caesar, P. D.; Meisel, S. L.; Offenhauer, R. D. Distribution of Nitrogen in Petroleum According to Basicity. *Ind. Eng. Chem.* **1952**, *44*, 2601−2605.
(59) Babarao, R.; Dai, S.; Jiang, D.-e. Functionalizing Porous Aromatic Frameworks with Polar Organic Groups for High-Capacity and Selective CO_2 Separation: A Molecular Simulation Study. *Langmuir* **2011**, *27*, 3451−3460.
(60) Torrisi, A.; Bell, R. G.; Mellot-Draznieks, C. Functionalized MOFs for Enhanced CO_2 Capture. *Cryst. Growth Des.* **2010**, *10*, 2839−2841.
(61) Liu, Y.; Wilcox, J. Effects of Surface Heterogeneity on the Adsorption of CO_2 in Microporous Carbons. *Environ. Sci. Technol.* **2012**, *46*, 1940−1947.
(62) Herm, Z. R.; Krishna, R.; Long, J. R. CO_2/CH_4, CH_4/H_2 and $CO_2/CH_4/H_2$ Separations at High Pressures Using Mg_2(dobdc). *Microporous Mesoporous Mater.* **2012**, *151*, 481−487.
(63) Patel, H. A.; Hyun Je, S.; Park, J.; Chen, D. P.; Jung, Y.; Yavuz, C. T.; Coskun, A. Unprecedented High-Temperature CO_2 Selectivity in N_2-Phobic Nanoporous Covalent Organic Polymers. *Nat. Commun.* **2013**, *4*, 1357.

DOI: 10.1021/acsami.6b00567
ACS Appl. Mater. Interfaces 2016, 8, 8491−8501